# Stabilization Principles for Polar Surfaces of ZnO

Jeppe V. Lauritsen,[†,*] Soeren Porsgaard,[†] Morten K. Rasmussen,[†] Mona C. R. Jensen,[†] Ralf Bechstein,[†] Kristoffer Meinander,[†] Bjerne S. Clausen,[‡] Stig Helveg,[‡] Roman Wahl,[§] Georg Kresse,[§] and Flemming Besenbacher[†]

[†]Interdisciplinary Nanoscience Center (iNANO) and Department of Physics and Astronomy, Aarhus University, Denmark, [‡]Haldor Topsøe A/S, Nymøllevej 55, Lyngby Denmark, and [§]Faculty of Physics, University of Vienna and Centre for Computational Materials Science, Sensengasse 8/12, 1090 Wien, Austria

**ABSTRACT** ZnO is a wide band gap metal oxide with a very interesting combination of semiconducting, transparent optical and catalytic properties. Recently, an amplified interest in ZnO has appeared due to the impressive progress made in nanofabrication of tailored ZnO nanostructures and functional surfaces. However, the fundamental principles governing the structure of even the clean low-index ZnO surfaces have not been adequately explained. From an interplay of high-resolution scanning probe microscopy (SPM), X-ray photoelectron spectroscopy (XPS), near edge X-ray absorption fine structure (NEXAFS) spectroscopy experiments, and density functional theory (DFT) calculations, we identify here a group of hitherto unresolved surface structures which stabilize the clean polar O-terminated ZnO(000$\bar{1}$) surface. The found honeycomb structures are truly remarkable since their existence deviates from expectations using a conventional electrostatic model which applies to the opposite Zn-terminated (0001) surface. As a common principle, the differences for the clean polar ZnO surfaces are explained by a higher bonding flexibility of the exposed 3-fold coordinated surface Zn atoms as compared to O atoms.

**KEYWORDS:** zinc oxide · polar surfaces · metal oxides · noncontact atomic force microscopy · surface hydroxylation · catalysis

**S**olid ionic compounds, built by stacking charged atomic layers, expose surfaces that are *polar* when there is a finite dipole moment in the repeat unit cell perpendicular to the surface.[1,2] Polar surfaces formed by a direct truncation of the crystal lattice are, however, unstable due to a diverging electrostatic energy and the surface must therefore be energetically compensated by adopting a modified or reconstructed surface structure. A proto-typical, but still poorly understood, material exposing polar surfaces is zinc oxide (ZnO). ZnO is a wide band gap metal oxide with an interesting combination of tunable semiconducting and transparent optical properties and has a very wide range of applications in areas such as optoelectronics, photovoltaics, light emitting devices, catalysis, and gas sensors.[3] Recently, an increased interest in ZnO has appeared due to the substantial progress made in nanofabrication methods, which has led to the synthesis of a multitude of tailored ZnO nanostructures and surfaces with interesting and unique functional properties.[4−6] When a wurtzite ZnO crystal (Figure 1a) is sliced perpendicular to the (0001)-axis, two principally different polar surfaces that are both exposed in natural crystals, termed the Zn-terminated ZnO(0001) and the O-terminated ZnO(000$\bar{1}$) surface, are formed (Figure 1a). Electrostatic considerations predict that the removal of *a quarter* of the surface ions ($O^{2-}$ for ZnO(000$\bar{1}$) and $Zn^{2+}$ for ZnO(0001)) will nullify the resulting dipole and result in stable nonpolar surfaces of this type. The exact structure of both ZnO(0001)-type surfaces and the implications for surface stability are, however, still being debated intensively.[7−15] For the Zn-terminated (0001) surface, scanning tunnelling microscopy (STM) in combination with density functional theory (DFT) have revealed that the surface is stabilized by the spontaneous formation of a high concentration of Zn-deficient triangular pits and step edges terminated by under-coordinated O atoms.[16,17] Since the formation of these pits is driven entirely by *electrostatics*, that is, the Madelung energy of large Zn deficient pits is lower than for isolated Zn vacancies, one would expect similar O-deficient structures to form on the O-terminated ZnO(000$\bar{1}$) surface. However, scanning probe microscopy studies have been unable to reveal the detailed atomic-scale structure of the O-terminated ZnO(000$\bar{1}$) surface and a detailed understanding of the surface morphology of the O-terminated ZnO(000$\bar{1}$) surface, and its relation to the opposite Zn-terminated surface, has been missing. In this report we reveal surprisingly that the compensation mechanism is fundamentally different on the O-terminated surface. Instead of the expected corrugated morphology, the O-terminated ZnO(000$\bar{1}$) surface is flat and exposes a group of previously unresolved (2 × 2)
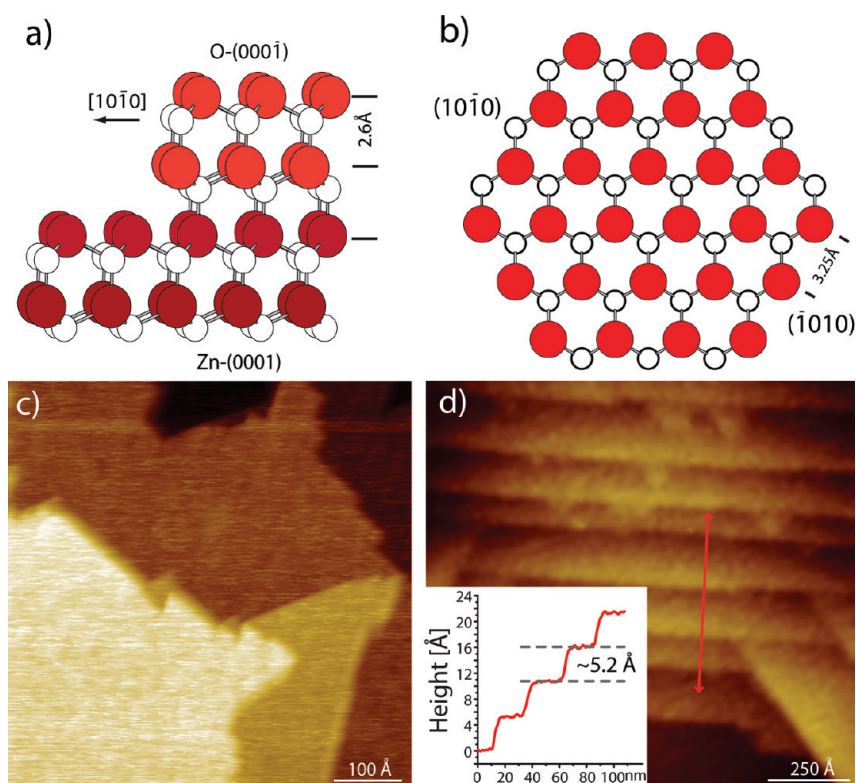
**Figure 1.** (a) Bulk ZnO crystallizes in the wurtzite structure and adopts alternating hexagonal planes of 4-fold coordinated Zn and O atoms, forming Zn—O—Zn—O layers. The ball model (side view) shows the wurtzite ZnO structure with a 2-fold ZnO step (Zn, white; O, red). (b) Hypothetical hexagonal slab of a bulk truncated O-terminated ZnO(000$\bar{1}$) slab exposing the two different low-index edges. (c) STM image (600 × 600 Å$^2$) of ZnO(000$\bar{1}$) at 450 °C. (d) Topographic NC-AFM image of a more stepped region at room-temperature (1200 × 1200 Å$^2$).

and (5 × 5) honeycomb surface structures. The new surface structures consist of alternating patches of the regular wurtzite and an unconventional zinc-blende ZnO stacking separated by double-layer holes which stabilize the surface in a wide range of the surface phase diagram as modeled by DFT. The basic difference between the two ZnO(0001)-type surfaces has a simple explanation related to the bonding preferences of Zn and O. Whereas oxygen prefers a tetrahedral or pyramidal bonding configuration, the 3d element Zn is more flexible with respect to bond formation. The present results clearly demonstrate that electrostatics alone do not drive the surface reconstructions of an ionic material like ZnO[10,16,17] and that models based only on simple ion rejection do not stabilize the surface as previously anticipated. The new insight presented for the O-terminated ZnO(000$\bar{1}$) surface may have implications for how polar surface reconstructions in general should be modeled.

## RESULTS AND DISCUSSION

Previously, STM studies have not been able to reveal direct atomic-scale information on the structure of the O-terminated ZnO(000$\bar{1}$) surface, since the surface is too weakly conducting at room temperature. Here we overcome the difficulty of characterizing the morphology of the O-terminated ZnO(000$\bar{1}$) surface by using an integrated variable-temperature STM and atom-resolved noncontact atomic force microscopy (NC-AFM) setup. NC-AFM is suitable for atomic-scale imaging of any flat surface irrespective of the substrate conductivity.[18] Furthermore, by switching the operation to the STM mode at elevated sample temperature, the substrate conductivity is increased sufficiently to record high-resolution STM images, hence providing a full characterization of the surface both at room temperature and elevated temperatures. Both NC-AFM images of the ZnO(000$\bar{1}$) surface at room temperature and elevated temperature STM images reveal a flat surface (Figure 1c) with relatively large terraces, which are, however, interrupted by high step density regions (Figure 1d). As illustrated in the inserted line scan in Figure 1d, the majority of the step edges are ∼5.2 Å high corresponding to two layers of ZnO (Figure 1a). Such 2-fold step edges are terminated by sequentially stacked O-terminated ($\bar{1}$010) edges and Zn-terminated (00$\bar{1}$0) edges (Figure 1b) and are therefore stoichiometric with respect to the Zn:O ratio, which, in a tentative model excluding vacancies on the edges, agrees with the observation that surface roughness does not significantly contribute to the stabilization on the O-terminated surface.[8] This finding is in distinct contrast to the opposite Zn-terminated surface, where very corrugated structures consisting of single-layer
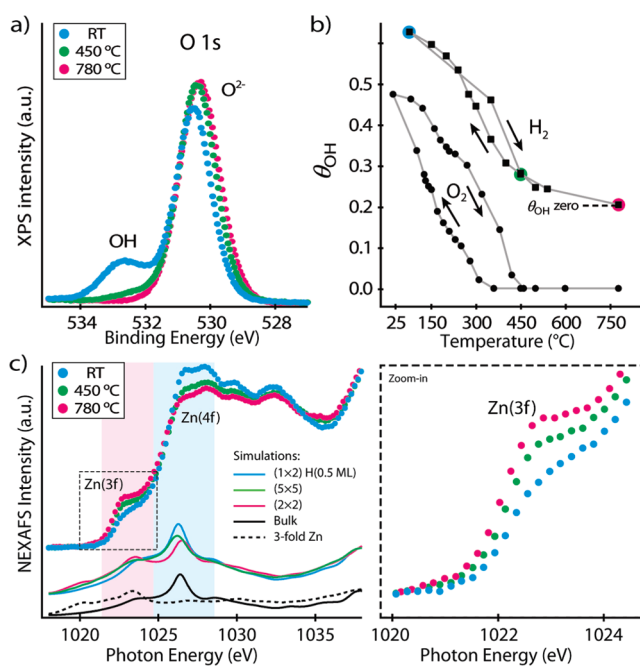
**Figure 2.** (a) O1s XPS spectra of the ZnO(000$\bar{1}$) surface. The OH peak is used to quantify $\theta_{OH}$ by varying the photon energy. (b) $\theta_{OH}$ as a function of $T$ in $H_2$ ($P = 5 \times 10^{-5}$ mbar) and $O_2$ ($P = 5 \times 10^{-7}$ mbar) gas. Arrows indicate heating and cooling. For clarity the zero-point coverage in $H_2$ is shifted. (c) L-edge NEXAFS spectra of the ZnO(000$\bar{1}$) surface recorded at three different temperatures (full circles). Thin lines correspond to the theoretical partial density of empty Zn s- and d-states.[24] To account for the experimental broadening, the theoretical DOS were folded by a Lorentzian function ($\gamma = 1.0$). Contributions from each layer have been weighted to account for the electron escape depth.

triangular pits and O-terminated step edges stabilize the surface.[16,17,19] Instead the O-terminated surface must be stabilized by other mechanisms.

Electrostatic arguments suggest that the plain ZnO-(000$\bar{1}$) surface may be stabilized by adding 0.5 monolayer (ML) of H which exist as terminal hydroxyl (OH) groups on the otherwise unreconstructed (1 × 1) ZnO surface.[10] In agreement, our XPS spectra and several previous studies (ref 7 and 20 and references therein) reveal the presence of a substantial amount of OH groups on the ZnO(000$\bar{1}$) surface at lower temperatures even under UHV conditions. Residual $H_2$ and $H_2O$ gases[7] and bulk H[21,22] cannot be neglected even under excellent UHV conditions and they can easily be the source of H on our ZnO sample. In fact, recent positron annihilation spectroscopy measurements confirm that commercially available ZnO crystals possess significant amounts of Zn-vacancy hydrogen complexes.[22] In our studies, the coverage ($\theta_{OH}$) was quantified by depth profile XPS measurements of the main O(1s) photoemission peak (530.4 eV) and a shifted energy peak (532.3 eV) which uniquely reflects OH-groups on the surface[7,23] as shown in Figure 2a. On the basis of the depth profile XPS measurement at room temperature, $\theta_{OH}$ had a saturation value of 0.49 ± 0.08 ML independent of whether the ambient is $O_2$ or $H_2$ at low pressures or UHV, which again suggests a bulk H source. This saturation coverage is in full accordance with the theoretical prediction that the addition of 0.5 ML of H on a stoichiometric (1 × 2)H-ZnO(000$\bar{1}$)-surface

(Figure 4a) leads to a stable surface when H is present.[10] The first direct space evidence for a well-ordered H-adsorbate layer on the ZnO(000$\bar{1}$) surface, is provided by our atom-resolved NC-AFM image of the ZnO(000$\bar{1}$) surface under the same conditions as the XPS experiment. The NC-AFM image in Figure 3a is atomically resolved and reveals the structure of the ZnO(000$\bar{1}$) surface in this state as an atomic row-like structure with a periodicity of 5.6 ± 0.2 Å in the direction perpendicular to the stripes. This row structure is clearly compatible with the calculated (1 × 2)H adsorbate structure (Figure 4a) which is calculated to fully stabilize the ZnO(000$\bar{1}$) surface at room temperature.

The plot in Figure 2b, however, reveals that $\theta_{OH}$ drops significantly as the sample is heated slightly above room temperature. This is in agreement with previous XPS[7,20] and thermal desorption spectroscopy studies,[21] and a completely hydrogen-free ZnO(000$\bar{1}$) surface can be obtained at temperatures in excess of 500 °C (Figure 2b). The hysteresis for the heating and cooling isobars in $O_2$ (Figure 2b) is explained by kinetic effects involved in the formation of the surface OH groups. The high-resolution STM image in Figure 3b was recorded at ∼450 °C just before complete dehydroxylation was achieved, and the STM image indeed reveals the presence of an atomic-scale reconstruction on the terrace planes, which replaces the stabilizing effect of H. The reconstruction is characterized by a rhombic unit cell with a depression defining the corners surrounded by six protrusions (Figure 3c). The
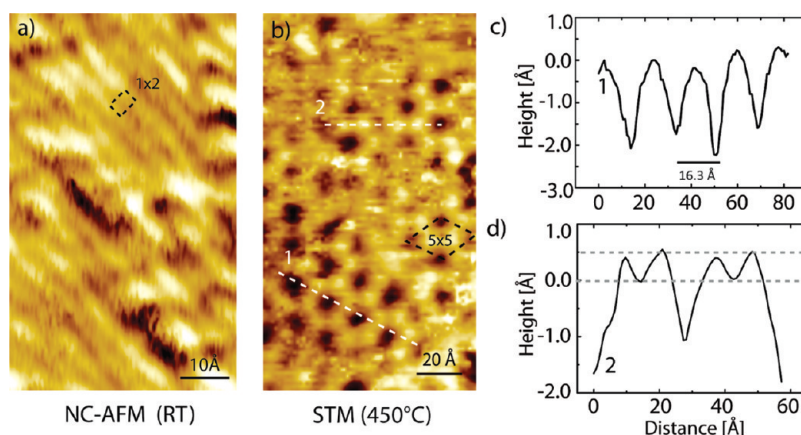
**Figure 3.** (a) High-resolution, constant height NC-AFM image (50 × 80 Å², $V_{CP}$ = 4.3 V, $\Delta f_{set}$ = −111 Hz) of the H-covered surface ZnO(000$\bar{1}$) in the (1 × 2) H-covered state at room temperature. (b) High-resolution STM image (110 × 180 Å²) of the honeycomb (5 × 5) reconstructed structure present on the terrace planes (imaging parameters at 450 °C, $V_t$ = 3.1 V, $I_t$ = 1.8 nA). The (5 × 5) unit cell is indicated by the rhombus. Line scans are indicated by the white dashed lines. (c) Line scan 1 illustrates the 16.3 Å periodicity of the 5 × 5 unit cell and the 2.1 Å depth of the dark holes. (d) Line scan 2 illustrates the corrugation across a pair of protrusions.
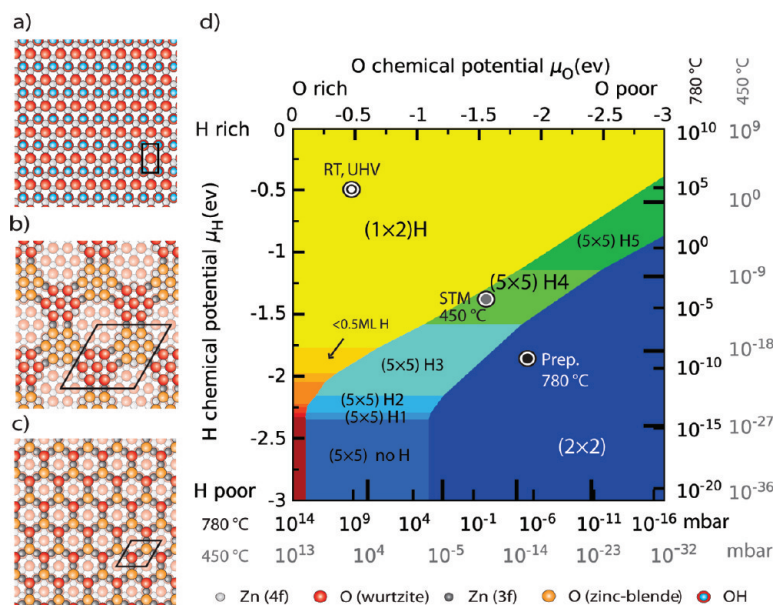


**Figure 4.** Schematic ball models of the stable structures considered for the calculation of the surface phase diagram of the O-terminated ZnO(000$\bar{1}$)-surface. (a) ZnO(000$\bar{1}$)-(1 × 2) OH-covered with 0.5 ML H, (b) ZnO(000$\bar{1}$)-(5 × 5), and (c) ZnO(000$\bar{1}$)-(2 × 2) surfaces. The positions of four- and three-fold coordinated Zn atoms are indicated by light (Zn(4f)) and dark (Zn(3f)) gray balls, respectively. (d) Surface phase diagram for the O-terminated ZnO(000$\bar{1}$)-surface as a function of O and H chemical potentials. The (5 × 5)-H$n$ notation refers to the number of adsorbed hydrogen ($n$) per (5 × 5) unit cell. For conversion to pressure, the black and gray scales indicate a temperature of 780 and 450 °C, respectively. Preparation conditions (black point), $T$ = 780 °C, $P_{O_2}$ = 5 × 10⁻⁷ mbar and $P_{H_2}$ = ∼1 × 10⁻⁹ mbar). STM in UHV conditions (gray point): $T$ = 450 °C, $P_{O_2}$ = 1 × 10⁻¹¹ mbar and $P_{H_2}$ = 1 × 10⁻¹⁰ mbar.

dimension of the unit cell is 16.3 ± 0.02 Å, which is five times the length of the in-plane unit cell ($a$ = 3.25 Å, see Figure 1b), and the observed honeycomb pattern can thus be interpreted as a (5 × 5) reconstruction. Line scans in the STM images reveal two characteristics of the atomic structure of the ZnO(000$\bar{1}$)-(5 × 5) structure: (i) The average corrugation of the depression relative to the protrusions is approximately 2.1 Å (Figure 3c). This rather high corrugation is tentatively attributed to the height of a single ZnO step (2.6 Å in

Figure 1a), and (ii) the line scan in Figure 3d shows that the pairs of bright protrusions surrounding the dark depression exhibit a corrugation of 0.4 ± 0.1 Å relative to the region in between them.

To explore the thermodynamic stability of the ZnO-(000$\bar{1}$) surface, we have performed extensive DFT calculations. A large number of structural models compatible with the experimentally observed (5 × 5) structure were first investigated using the following conditions: (i) a partial removal of a Zn−O layer, (ii) an
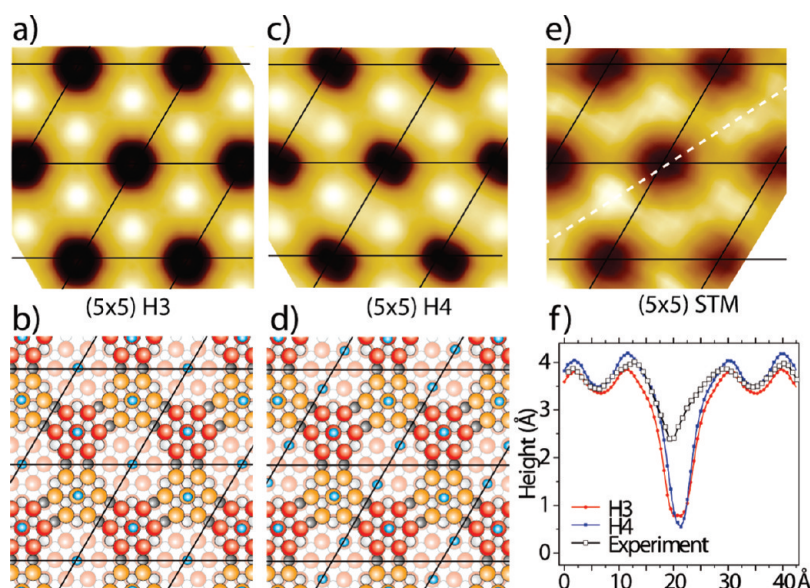
**Figure 5.** (a) Simulated STM images and (b) ball structure model (top view) of the ($5 \times 5$) structure with three OH groups per unit cell (H3). Red balls reflect O in the regular wurtzite stacking, whereas orange reflect O atoms in a zinc-blende stacking. Small blue balls indicate H atom positions. (c) Simulated STM image and (d) ball structure model of the ($5 \times 5$) structure with four H per unit cell (H4). (e) Correlation averaged experimental STM image. (f) Line scans corresponding to the white dashed line in the STM images and simulations of H3 and H4. Other configurations are shown in the Supporting Information.

approximate 6-fold symmetry axis in the center of the hexagonal holes, and (iii) the removal of approximately one-quarter of the surface oxygen atoms in order to stabilize the surface electrostatically. In Figure 4b we show a ball model of the most stable ($5 \times 5$) structure resulting from this analysis. The structure is constructed by removing 11 O atoms and 7 Zn atoms from the topmost layer of the ($5 \times 5$) unit cell, which results in a single layer deep hexagonal hole. In the topmost surface layer, 7 O atoms are bonded by 4-fold coordinated Zn(4f) atoms to form hexagons, and two such hexagons, one in the regular wurtzite ZnO stacking sequence (red balls) and one in an atypical zinc-blende stacking sequence (orange balls), are interlinked by six 3-fold coordinated Zn(3f) atoms (gray balls) to form a honeycomb-like structure. Formally this ($5 \times 5$) structure is still polar, since a nonpolar structure requires the removal of one-quarter of the oxygen surface atoms ($\sim$6 out of 25 in a ($5 \times 5$) unit cell), whereas only 4 more O than Zn atoms are removed in the present model. The remaining partial polarity of the ($5 \times 5$) structure can be compensated by the formation of hydroxyl groups on the surface. By adding neutral H on top of O atoms in our model, we indeed find a family of more stable structures incorporating up to 5 OH groups per ($5 \times 5$) unit cell (see Supporting Information). Figure 5 panels a–e show a direct comparison of the experimental STM image and two STM simulations for the predicted ($5 \times 5$) structure with three and four OH groups, respectively, corresponding to a hydroxyl coverage of $\theta_{OH}$ = 0.12–0.16 ML. Excellent quantitative and qualitative correlation between experimental corrugation and simulations is obtained for these

configurations as is depicted in Figure 5f. The hydrogen-free ($5 \times 5$) surface and the other H coverages did not match the STM image (see Supporting Information). Instead, the most stable hydrogen-free structure identified in the DFT calculations is a stoichiometric ($2 \times 2$) structure (Figure 4c) constructed from the same principles as the ($5 \times 5$) structure. It is obtained by removing two O and one Zn atom in a ($2 \times 2$) unit cell and shifting the position of one O atom (orange) to the zinc-blende site. In this way, the ($2 \times 2$) structure fully compensates for the surface dipole without the need for H adsorbates. The O atoms on the surface are interlinked by three corner-shared Zn atoms (dark gray balls), which all obtain an unusual 3-fold coordination to O (Figure 4c).

The key distinguishing feature between the ($1 \times 2$)H, ($5 \times 5$), and ($2 \times 2$) surface structures (Figure 4a–c) is the relative number of 3-fold coordinated Zn(3f) atoms to Zn(4f) on the surface. We have studied the formation of such Zn-species as a function of sample conditions with near edge X-ray absorption fine structure (NEXAFS) spectroscopy. NEXAFS measures variations in the X-ray absorption coefficient[24] and in the present case the NEXAFS data from the Zn L-edge closely resemble the local s and d density of state (DOS) of the Zn atoms in the surface region. Our NEXAFS spectra recorded under the conditions corresponding to the three main surface structures (room temperature, 450 °C in UHV, and 780 °C in $O_2$, respectively) and matching NEXAFS simulations based on the Zn-projected DOS for the ($1 \times 2$)H, ($5 \times 5$), and ($2 \times 2$) structures, respectively, are illustrated in Figure 2c. In this figure is also depicted a calculated reference spectrum for Zn(4f) in bulk ZnO

which has a strong main peak at ~1027 eV, whereas the main peak of Zn(3f) atoms is a broader feature at ~1023 eV. At room temperature, the NEXAFS spectroscopy curve in Figure 2c is dominated by Zn(4f) species. However, at 450 °C, a strong Zn(3f) feature develops as a shoulder around 1022 eV (see zoom-in for Figure 2c), and at the same time the main Zn(4f) feature at 1027−28 eV drops considerably in intensity, indicating the formation of the (5 × 5) phase. This trend is further amplified at high temperature (780 °C) and fully supports the existence of the hydrogen-free (2 × 2) phase with Zn(3f) surface species.

To finally construct a complete phase diagram for the ZnO(000$\bar{1}$) surface, we have calculated the stability of the surfaces, and Figure 4d depicts the most stable structures as a function of the chemical potential of hydrogen and oxygen. We have also evaluated the new structures against the stability of large triangular, one layer deep pits, which are the prevalent structures on the opposite Zn-terminated ZnO(0001) surface.[17] Although pits are preferred over isolated O vacancies,[9] the (2 × 2) and (5 × 5) structures are predicted to be even more stable under reducing conditions, whereas the (1 × 2)H surface dominates at high oxygen and hydrogen pressures and relatively low temperatures. The condition under which STM was performed (450 °C, UHV) is indicated by an open gray circle, and it is concluded that these conditions indeed reflect a ZnO surface with a (5 × 5) structure and 4 OH groups per unit cell (H4), which is again in full agreement with the H content revealed from the STM simulation and in correspondence with the experimentally determined value of $\theta_{OH}$ at this temperature (Figure 2b). At high temperatures corresponding to the preparation conditions of this experiment (780 °C, black pressure scale), the hydrogen-free (2 × 2) phase is predicted to dominate. From the isobar plots in Figure 2b the phase transition from the (5 × 5) structure to the (1 × 2)H is observed in the experiment to occur around 300 °C, where the surface mobility of Zn is likely to be high enough to still facilitate the restructuring of the Zn positions.

It is interesting to observe that the predominant surface structures present on the two related polar (0001) and (000$\bar{1}$) surfaces are so fundamentally different. To substantiate this point, we have re-examined the Zn-terminated ZnO(0001) phase diagram including the new models of the (000$\bar{1}$) surface in Figure 4b,c, with Zn and O atoms interchanged. We found that the inclusion of these models did not change the previous results for the Zn-terminated ZnO(0001) phase diagram.[17] The basic difference between the two ZnO surfaces has a simple explanation related to the specific bonding preferences of Zn and O atoms. Oxygen prefers a tetrahedral or pyramidal bonding configuration, in which case all three O 2p orbitals can interact to form bonding and antibonding linear combinations, whereas the 3d element Zn is more flexible with
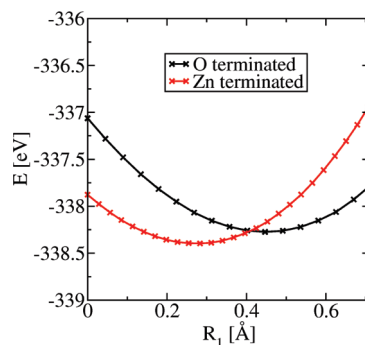


**Figure 6.** Dependence of the total energy on the height $R_1$ of surface Zn and O atoms of a nonpolar (compensated) ZnO-(0001) and ZnO(000$\bar{1}$) surface where every fourth Zn or O atom is removed from the surface, respectively. Since the surface is electrostatically compensated and locally stoichiometric, each Zn and O atom is fully ionized (Zn$^{2+}$, O$^{2-}$). The Zn$^{2+}$ ions are located in a more planar configuration and protrude only 0.3 Å above the second layer O$^{2-}$ ions, whereas O$^{2-}$ ions are located 0.5 Å above the second layer Zn$^{2+}$ ions. A planar configuration is very unfavorable for O$^{2-}$.

respect to bond formation. In the pyramidal configuration, the out of plane $d_{xz}$ and $d_{yz}$ orbitals dominate, while for flat or planar bond situations the $d_{xy}$ and $d_{x^2-y^2}$ orbitals contribute. This effect can be demonstrated by a simple DFT model calculation of the total energy of a (0001) and (000$\bar{1}$) surface as a function of displacement of the outermost Zn and O atom for a nonpolar reconstruction (Figure 6). The Zn$^{2+}$ ions sink much deeper into the surface than the O$^{2-}$ ions: O ions clearly prefer a pyramidal coordination, protruding typically 0.5 Å above the three neighboring Zn ions on the (000$\bar{1}$) surface, whereas the equivalent Zn ions are much more free to relax and typically protrude only by 0.3 Å on the (0001) surface. The flexibility of the Zn coordination is essential for the observed stability of the (5 × 5) and (2 × 2) structures, since a third or all of the surface Zn atoms, respectively, are placed in a flat Zn(3f) configuration with three neighboring O atoms being coplanar with the Zn atom (Figure 2b,c). On the Zn-terminated (0001) surface, hypothetical (5 × 5) and (2 × 2) structures would force O into a coplanar configuration with three neighboring Zn atoms, which is energetically very much more unfavorable than the opposite situation (Figure 6).

## CONCLUSION

The existence of the (5 × 5) and (2 × 2) structures on the ZnO(000$\bar{1}$) surface thus provides new fundamental insight into the mechanism governing the cancellation of surface polarity on ZnO(0001) surfaces, and the results demonstrate that more elaborate models which include larger atomic relaxations must be added to the conventional and widely applied models based on cancelation of the dipole by the partial removal of atoms from their bulk positions.[1,2] Such a model should be applicable for the analysis of the atomic-scale structures and stability of other polar surfaces

from the large and important group of ionic compounds (*e.g.*, oxides, sulfides), which consists of transition metals, with a bonding flexibility similar to that of Zn, in combination with lighter anions with a strict preferential *p*-type bonding, such as O. Additionally, the present findings demonstrate how the ZnO surface structures may respond dynamically to changes in the surrounding ambient atmosphere at elevated temperature. The synthesis of new functional ZnO nanostructures may greatly benefit from such insight since it often relies on a detailed knowledge of growth on selected ZnO facets and an exact atomic-scale understanding of, for example, adhesion on metals or other metal oxides. The detailed surface phase diagrams now established for ZnO surfaces may also facilitate a better atomistic understanding of the intriguing dynamic effects previously observed for Cu/ZnO catalysts, where the catalytic activity of methanol formation correlates directly with dynamic and reversible morphology changes of the ZnO-supported Cu nanoparticles induced by a shift from oxidizing to reducing conditions.[25−28]

## MATERIALS AND METHODS

**Materials.** Polished O-terminated ZnO(000$\bar{1}$) crystals (MTI Corporation, Richmond, USA) were cleaned *in situ* by a large number of preparation cycles (>20) involving 1 keV Ar$^+$ ion bombardment followed by annealing for 15 min to 780 °C in 5 × 10$^{-7}$ mbar of O$_2$. The annealing performed in an oxygen atmosphere was found to be beneficial for the preparation of a flat surface after sputtering.

**Scanning Probe Microscopy.** SPM was performed in an ultrahigh vacuum (UHV) chamber (base pressure $P = 1 \times 10^{-10}$ mbar) using a variable-temperature AFM/STM (Omicron Nanotechnology). At room temperature the conductivity of the clean O-terminated ZnO surface was too low to allow high-resolution STM, but by heating the sample to ∼450 °C high-resolution STM images could be obtained. Heating in the STM was achieved by passing a current of ∼0.5 A through a doped Si-strip clamped on the backside of the ZnO crystal. $V_t$ denotes the tunneling bias, and $I_t$ denotes the tunneling current. For characterization at lower temperature where the ZnO surface was found to be insulating, atomic force microscopy was performed in the noncontact mode (NC-AFM) by oscillating the cantilever at constant amplitude (∼20 nm) at its first resonance frequency and using the frequency detuning ($\Delta f$) as feedback signal to record topographic images. Nanosurf EasyPLL Plus electronics (Liestal, Switzerland) were used for FM-demodulation in the NC-AFM mode. Atom-resolved NC-AFM images were recorded in the constant height mode,[29] in which case the corrugation in the NC-AFM reflects variation in the $\Delta f$ relative to a preset value $\Delta f_{set}$ as the tip scans the surface. Silicon cantilevers (Nanosensors, NCH-type) with a resonance frequency of 260 kHz were used, and for STM, etched W tips were used. The contact potential (CP) difference between sample and tip was monitored before the experiment started and electrostatic forces were compensated by applying a bias ($U_{CP}$) between tip and sample.

**Photoemission Spectroscopy.** The X-ray photoelectron spectroscopy (XPS) and near edge X-ray absorption fine structure (NEXAFS) spectroscopy experiments were performed at ambient pressure XPS beamline 11.0.2 of the Advanced Light Source (ALS), Lawrence Berkeley National Laboratory (LBNL). The end station (base pressure of 2 × 10$^{-10}$ mbar) consists of a preparation chamber and an analysis chamber equipped with a XPS analyzer with a differentially pumped electrostatic lens system that allows XPS measurements at elevated pressures. Zn L-edge NEXAFS was recorded in partial electron yield, counting emitted electrons with kinetic energy around 820 eV, by keeping a high pass energy. The incident beam was linearly polarized perpendicularly to the sample with an angle of incidence of 73°.

**Theoretical.** The density functional theory calculations were performed using the plane wave code VASP[30] and the projector augmented wave method in the implementation of G. Kresse and D. Joubert.[31] The energy cutoff was set to 280 eV, and the PW91 gradient corrected functional was used throughout the work.[32] Polarity of the inert Zn-terminated ZnO(0001) surface was removed by a suitable Zn-like pseudopotential with a fractional valency of 1.5. The *k*-point sampling was performed using similar grids as described in ref 17. Specifically, for the (5 ×

5) unit cell, a Γ centered 2 × 2 *k*-point grid was used. The phase diagram was calculated from DFT energies using the methods described in ref 17. Constant current STM images were simulated using the model of Tersoff and Hamann by plotting contours of the local density of states projected onto the tip apex.[33] The Zn L-edge NEXAFS spectroscopy curves were simulated from the DFT calculations by determining the partial density of empty Zn s- and d-states.[24] We have neglected multiplet effects since the 3d-band in Zn is filled. To account for the escape depth of the photoelectrons in NEXAFS, the individual contributions from layers are weighted using a weighting coefficient of 1.0 (top layer), 0.6 (second layer), and 0.3 (third layer). The qualitative features are however insensitive to the exact weighting coefficients. The final density of states is folded using a Lorentzian function ($\gamma = 1.0$) to account for the experimental broadening.

*Supporting Information Available:* Detailed comparison of STM experiments and simulations of the (5 × 5) reconstruction on the O-terminated ZnO(000$\bar{1}$) for all hydrogen coverages. This material is available free of charge *via* the Internet at http://pubs.acs.org.

## REFERENCES AND NOTES

1. Goniakowski, J.; Finocchi, F.; Noguera, C. Polarity of Oxide Surfaces and Nanostructures. *Rep. Prog. Phys.* **2008**, *71*, 016501.
2. Tasker, P. W. Stability of Ionic-Crystal Surfaces. *J. Phys. C* **1979**, *12*, 4977–4984.
3. Ellmer, K.; Klein, A.; Rech, B. *Transparent Conductive Zinc Oxide: Basics and Applications in Thin Film Solar Cells*, 1st ed.; Springer: Berlin, 2008; p 443.
4. Wang, Z. L. Splendid One-Dimensional Nanostructures of Zinc Oxide: A New Nanomaterial Family for Nanotechnology. *ACS Nano* **2008**, *2*, 1987–1992.
5. Schmidt-Mende, L.; MacManus-Driscoll, J. L. ZnO—Nanostructures, Defects, and Devices. *Mater. Today* **2007**, *10*, 40–48.
6. Wang, Z. L.; Song, J. H. Piezoelectric Nanogenerators Based on Zinc Oxide Nanowire Arrays. *Science* **2006**, *312*, 242–246.

7. Wöll, C. The Chemistry and Physics of Zinc Oxide Surfaces. *Prog. Surf. Sci.* **2007**, *82*, 55–120.

8. Dulub, O.; Boatner, L. A.; Diebold, U. STM Study of the Geometric and Electronic Structure of ZnO(0001)-Zn, (000$\bar{1}$)-O, (10$\bar{1}$0), and (11$\bar{2}$0) Surfaces. *Surf. Sci.* **2002**, *519*, 201–217.

9. Meyer, B.; Marx, D. Density-Functional Study of the Structure and Stability of ZnO surfaces. *Phys. Rev. B* **2003**, *67*, 035403.

10. Meyer, B. First-Principles Study of the Polar O-Terminated ZnO Surface in Thermodynamic Equilibrium with Oxygen and Hydrogen. *Phys. Rev. B* **2004**, *69*, 045416.

11. Wander, A.; Schedin, F.; Steadman, P.; Norris, A.; McGrath, R.; Turner, T. S.; Thornton, G.; Harrison, N. M. Stability of Polar Oxide Surfaces. *Phys. Rev. Lett.* **2001**, *86*, 3811–3814.

12. Valtiner, M.; Todorova, M.; Grundmeier, G.; Neugebauer, J. Temperature Stabilized Surface Reconstructions at Polar ZnO(0001). *Phys. Rev. Lett.* **2009**, *103*, 065502.

13. Lindsay, R.; Muryn, C. A.; Michelangeli, E.; Thornton, G. ZnO(000$\bar{1}$)-O Surface Structure: Hydrogen-Free (1 × 1) Termination. *Surf. Sci.* **2004**, *565*, L283–L287.

14. Overbury, S. H.; Radulovic, P. V.; Thevuthasan, S.; Herman, G. S.; Henderson, M. A.; Peden, C. H. F. Ion Scattering Study of the Zn and Oxygen-Terminated Basal Plane Surfaces of ZnO. *Surf. Sci.* **1998**, *410*, 106–122.

15. Jedrecy, N.; Sauvage-Simkin, M.; Pinchaux, R. The Hexagonal Polar ZnO(0001)-(1 × 1) Surfaces: Structural Features as Stemming from X-ray Diffraction. *Appl. Surf. Sci.* **2000**, *162*, 69–73.

16. Dulub, O.; Diebold, U.; Kresse, G. Novel Stabilization Mechanism on Polar Surfaces: ZnO(0001)-Zn. *Phys. Rev. Lett.* **2003**, *90*, 016102.

17. Kresse, G.; Dulub, O.; Diebold, U. Competing Stabilization Mechanism for the Polar ZnO(0001)-Zn Surface. *Phys. Rev. B* **2003**, *68*, 245409.

18. Morita, S.; Giessibl, F. J.; Wiesendanger, R. *Noncontact Atomic Force Microscopy*; Springer: Berlin, 2009.

19. Torbrügge, S.; Ostendorf, F.; Reichling, M. Stabilization of Zinc-Terminated ZnO(0001) by a Modified Surface Stoichiometry. *J. Phys. Chem. C* **2009**, *113*, 4909–4914.

20. Kunat, M.; Gil Girol, S.; Becker, T.; Burghaus, U.; Wöll, C. Stability of the Polar Surfaces of ZnO: A Reinvestigation Using He-Atom Scattering. *Phys. Rev. B* **2002**, *66*, 081402.

21. Qiu, H. S.; Meyer, B.; Wang, Y. M.; Wöll, C. Ionization Energies of Shallow Donor States in ZnO Created by Reversible Formation and Depletion of H Interstitials. *Phys. Rev. Lett.* **2008**, *101*, 236401.

22. Brauer, G.; Anwand, W.; Grambole, D.; Grenzer, J.; Skorupa, W.; Cizek, J.; Kuriplach, J.; Prochazka, I.; Ling, C. C.; So, C. K.; Schulz, D.; Klimm, D. Identification of Zn-Vacancy-Hydrogen Complexes in ZnO Single Crystals: A Challenge to Positron Annihilation Spectroscopy. *Phys. Rev. B* **2009**, *79*, 115212.

23. Yamamoto, S.; Bluhm, H.; Andersson, K.; Ketteler, G.; Ogasawara, H.; Salmeron, M.; Nilsson, A. *In Situ* X-ray Photoelectron Spectroscopy Studies of Water on Metals and Oxides at Ambient Conditions. *J. Phys. Condens. Matter* **2008**, *20*, 184025.

24. de Groot, F.; Kotani, A. *Core Level Spectroscopy of Solid*, 1st ed.; CRC Press: Boca Raton, Fl, 2008.

25. Clausen, B. S.; Schiøtz, J.; Gråbæk, L.; Ovesen, C. V.; Jacobsen, K. W.; Nørskov, J. K.; Topsøe, H. Wetting/Non-wetting Phenomena during Catalysis: Evidence From *in Situ* On-Line EXAFS Studies of Cu-Based Catalysts. *Top. Catal.* **1994**, *1*, 367–376.

26. Ovesen, C. V.; Clausen, B. S.; Schiotz, J.; Stoltze, P.; Topsøe, H.; Nørskov, J. K. Kinetic Implications of Dynamical Changes in Catalyst Morphology During Methanol Synthesis over Cu/ZnO Catalysts. *J. Catal.* **1997**, *168*, 133–142.

27. Hansen, P. L.; Wagner, J. B.; Helveg, S.; Rostrup-Nielsen, J. R.; Clausen, B. S.; Topsøe, H. Atom-Resolved Imaging of Dynamic Shape Changes in Supported Copper Nanocrystals. *Science* **2002**, *295*, 2053–2055.

28. Grunwaldt, J.-D.; Molenbroek, A. M.; Topsøe, N.-Y.; Topsøe, H.; Clausen, B. S. *In Situ* Investigations of Structural Changes in Cu/ZnO Catalysts. *J. Catal.* **2000**, *194*, 452–460.

29. Lauritsen, J. V.; Reichling, M. Atomic Resolution Non-contact Atomic Force Microscopy of Clean Metal Oxide Surfaces. *J. Phys. Condens. Matter* **2010**, *22*, 263001.

30. Kresse, G.; Furthmuller, J. Efficiency of *ab-Initio* Total Energy Calculations for Metals and Semiconductors Using a Plane-Wave Basis Set. *Comput. Mater. Sci.* **1996**, *6*, 15–50.

31. Kresse, G.; Joubert, D. From Ultrasoft Pseudopotentials to the Projector Augmented-Wave Method. *Phys. Rev. B* **1999**, *59*, 1758–1775.

32. Perdew, J. P.; Chevary, J. A.; Vosko, S. H.; Jackson, K. A.; Pederson, M. R.; Singh, D. J.; Fiolhais, C. Atoms, Molecules, Solids, and Surfaces: Applications of the Generalized Gradient Approximation for Exchange and Correlation. *Phys. Rev. B* **1992**, *46*, 6671–6687.

33. Tersoff, J.; Hamann, D. R. Theory of the Scanning Tunneling Microscope. *Phys. Rev. B* **1985**, *31*, 805–813.